Astron. Astrophys. 327, 681–688 (1997)

ASTRONOMY AND ASTROPHYSICS

The Na I resonance lines as a spectroscopic test of late-type stellar atmospheres⋆

A. Tripicchio[1], **G. Severino**[1], **E. Covino**[1], **L. Terranegra**[1], **and R.J. García López**[2]

[1] Osservatorio Astronomico di Capodimonte, Via Moiariello 16, I-80131 Naples, Italy
[2] Instituto de Astrofísica de Canarias, E-38200 La Laguna, Tenerife, Spain

Received 30 January 1997 / Accepted 11 June 1997

Abstract. We have tested current models for the atmospheres (including photosphere and low chromosphere) of late-type stars using the D resonance lines of neutral sodium as a diagnostic.

To this end, we have measured the equivalent widths of the D lines for a sample of 39 dwarf and 45 giant late-type stars observed with high spectral resolution. We constructed photospheric models over a grid in effective temperature and surface gravity spanning the spectral types F to M, and luminosity classes V and III of the sample stars. The model photospheres were extended into the chromosphere by assuming a suitable scaling from the Sun, and theoretical Na I D equivalent widths were computed over the grid of models including the deviations from local thermodynamic equilibrium.

By taking into account both the experimental errors and the possible variations of stellar parameters (effective temperature, surface gravity, sodium abundance and microturbulence), the comparison between observed and computed equivalent widths allows us to state that the model atmospheres we have used can reproduce the observations for the two luminosity classes and for all the spectral types except for the M-type stars. We have discussed the importance of line blanketing in the spectral analysis of these stars, but at present we cannot conclude that this effect would reduce the discrepancy.

Key words: line: formation – radiative transfer – stars: atmospheres – stars: chromospheres – stars: late-type

1. Introduction

The alkali spectra of the quiet Sun and plages on one hand, and of spot umbrae on the other, can be favourably compared with those of late F and late K to early M-type stars, respectively. Severino, Gomez & Caccin (1994) used the resonance lines of neutral alkalis to probe the Sun and found that the Na I resonance doublet at 5890 – 5896 Å (the D lines) is a sensitive temperature indicator for the upper photosphere and low chromosphere in solar spots. By extending these diagnostics to other late-type stars, Tripicchio et al. (1996) compared observed and synthetic spectra computed over a grid of model atmospheres corresponding to a wide range of effective temperatures and surface gravities and found, in a preliminary analysis, that current models work quite well for F-, G-, and K-type stars, while they do not for M-type stars.

The need for good modeling of stellar photospheres and the present status of the research in this field have recently been discussed by Gustafsson and Jørgensen (1994). In particular, with respect to the Na I D resonance lines, Covino et al. (1993) suggested that high signal-to-noise ratio (S/N) D-line profiles are important for late-type star modeling. Carrying to extremes the numerical fit of a portion of the stellar spectrum might help to interpret the residual differences between observations and calculations in terms of non-radiative heating in the stellar chromosphere. Andretta, Doyle & Byrne (1997) have studied the effect of chromospheric activity on the D lines in M dwarfs, and found that they can complement information given by other better-studied chromospheric lines, like the hydrogen Balmer series.

A more general motivation for this work is that the study of alkali lines in late-type stars might be helpful for the study of the formation of lithium lines in the atmospheres of these stars. In fact, while for sodium and potassium (which we will treat in a forthcoming paper to complement the spectroscopic diagnostic based on sodium) the derivation of abundances (based mainly on equivalent width measurements) would depend only on uncertainties associated with stellar activity, for lithium the scenario is more complex and its abundance depends also on other parameters such as rotation, spectral type, and the evolution of the star (e.g. Balachandran 1994; García López, Rebolo & Martín 1994, and references therein).

Send offprint requests to: A. Tripicchio

⋆ Based on observations collected at the European Southern Observatory (ESO), La Silla, Chile, and at the McDonald Observatory, Mt. Locke, Texas, USA.

The present paper is structured as follows: Sect. 2 describes the spectroscopic observations of the sodium D lines in a significant sample of late-type stars; Sect. 3 discusses the calculation of a grid of model atmospheres for these stars (including the photosphere and the low chromosphere), and the computation of Na I D-line equivalent widths taking into account the effects of non-local thermodynamic equilibrium (NLTE); in Sect. 4 we compare the observations with our model calculations, and Sect. 5 summarizes our main conclusions.

2. Observations and data analysis

High-resolution spectra of the Na I D lines for 84 late-type stars have been obtained during three different observing runs (between 1993 and 1995), using the 1.4-m Coudé Auxiliary Telescope (CAT) feeding the Coudé Echelle Spectrometer (CES) of the European Southern Observatory (ESO) at La Silla (Chile), and with the 2.7-m telescope of McDonald Observatory (Texas), also equipped with a coudé echelle spectrograph.

For most of the stars at least two independent exposures were taken during each observing run. These observations cover a wide range of the cool part of the HR diagram, both in spectral type (from F6 to M5), and luminosity class (V and III). Table 1 lists the stars observed, spectral types and V magnitudes, jointly with the exposure times and the equivalent widths of the sodium doublet (or its averages when two or more observations were available).

The CAT observations were conducted in two observing runs: 1993 July 31 to August 9, and 1995 March 12–16. In 1993, the CCD in use was an RCA SID 006 EX of 1024×640 pixels with a pixel size of 15 μm (ESO # 9), and the short camera configuration (red path) of the CES was used (Lindgren & Gilliotte 1989). In 1995, the CCD was a UV-coated LORAL of 2048×2048 pixels with a pixel size of 15 μm (ESO # 34), and the CES was operated in the long camera configuration. In both cases, the spectral range covered was about 50 Å, from 5870 to 5920 Å, centred on the Na I doublet. An entrance slit of 514 μm, corresponding to about 2 arcsec on the sky, was used yielding a nominal resolving power $\lambda/\Delta\lambda \sim 55000$. This was verified by measuring the full width at half maximum (FWHM) of well isolated lines on the Th-Ar comparison spectrum. The wavelength stability between subsequent exposures for the CES is very good, therefore the wavelength calibration was obtained from a single comparison spectrum for each night. For flat-fielding, average exposures of an internal quartz lamp were used. Our CAT observations were carried out in remote control from ESO headquarters in Garching. The exposure times ranged from 5 s, for 2.1 mag stars, up to 3600 s, for 8.5 mag stars. The achieved S/N was of 100 in the worst cases. The data reduction was performed using the MIDAS[1] package for the reduction of long-slit spectra following the standard procedure of bias subtraction, flat-fielding, and wavelength calibration.

The observations corresponding to the northern hemisphere were performed using the "2dcoudé" echelle spectrograph (Tull et al. 1995) at the 2.7-m Harlan Smith Telescope of the McDonald Observatory (Mt. Locke, Texas), in 1994 August. The detector employed was the AIS1 CCD (2048 × 2048 pixels), and the spectral resolution achieved with a ∼ 1-arcsec slit was $\lambda/\Delta\lambda \sim 60000$. Fifty spectral orders containing useful data were recorded, providing a spectral coverage from 4050 to 9700 Å with gaps between the orders. To allow a better correction of contamination by cosmic rays, we typically took three exposures with the same exposure time for each object, and the longest exposures employed were of 1800 s. The data reduction was carried out using the IRAF suite of programs[2], and consisted in bias and scattered light subtraction, flat-field correction, extraction of one-dimensional spectra, wavelength calibration, and continuum normalization. Individual spectra of a single object were coadded after extraction by weighted averaging or medianing. Wavelength calibration and linearization of the spectra were performed by comparison with exposures of a Th–Ar lamp obtained with the same instrumental configuration. Third-order polynomials were fitted to the data along the spectral and spatial directions, providing an rms scatter of 0.003 Å. The final dispersion for the 59$^{\rm th}$ order, corresponding to the Na I D doublet, was 0.041 Å/pixel.

The total equivalent width, W_λ, of the D lines was measured by means of a linear integration over the wavelength interval $\Delta\lambda$ (ranging from 14 to 40 Å for F5 to M5 stars) covered by the doublet; before doing that, the spectrum was cleared of all other lines not to be measured. In later spectral types, a problem associated with the presence of many spectral lines is the main difficulty for defining the local continuum in the spectral range observed. Errors in the location of the pseudo-continuum around the D lines therefore increase with advancing spectral type, introducing larger uncertainties in the equivalent width determinations. The experimental error, estimated by multiplying this uncertainty in locating the continuum by $\Delta\lambda$ is typically 0.1 dex for F-, G- and K-type stars but it can reach 0.3 dex for M-type stars.

3. Calculations

3.1. Model atmospheres

We computed photospheric models over a grid in effective temperature ($T_{\rm eff}$) and surface gravity (g) spanning the spectral types F to M, and the luminosity classes V and III covered by the sample stars.

The relationships $T_{\rm eff}$ and $\log g$ vs. spectral type and luminosity class used to build the grid, which is given in Table 2, were interpolated from Gray (1989). Other tables (Schmidt-Kaler 1982; Allen 1973), less complete than this one, have been also considered, and the comparison shows that the uncertainty

[1] MIDAS is distributed by ESO and the versions 92NOV and 95NOV, used for the reductions, are available at the Osservatorio Astronomico di Capodimonte.

[2] IRAF is distributed by National Optical Astronomy Observatories, which is operated by the Association of Universities for Research in Astronomy, Inc., under contract with the National Science Foundation, USA.

Table 1. List of observed stars. V (mag) is the visual magnitude in the Johnson UBV system. Columns 5-7 give the exposure times (s) of the spectra used for the data analysis, obtained during the 3 observing runs (see text). $\langle W_\lambda \rangle$ (Å) is the average equivalent width of the sodium doublet.

HD #	Other id.	Sp. type	V	Exposure time CAT 93	Exposure time CAT 95	Exposure time McD 94	$\langle W_\lambda \rangle$
3302	λ^2 Phe	F6 V	5.51	600			0.87
693	6 Cet	F7 V	4.89	600			0.73
7570	ν Phe	F8 V	4.96	600			1.25
27808		F8 V	7.14			1200 + 1800	1.28
141004	27 λ Ser	G0 V	4.36	180 × 2			1.13
212698	53 Aqr a	G1 V	6.35	1200			1.15
212697	53 Aqr b	G2 V	6.57	1200			1.31
219709		G2 V	7.34	2400			1.48
146233	18 Sco	G2 V	5.51	300			1.56
1835	9 Cet	G2.5 V	6.38			900 + 1200 × 2	1.72
195564	Gl 792.1 A	G3 V	5.65	600			1.46
220096	HR8883	G4 V	5.64	1200			1.59
214850	HR8631	G4 V	5.71			300 + 900 × 2	1.47
165185	Gl 702.1	G5 V	5.95	360 × 2			1.25
160691	μ Ara	G5 V	5.15	600			1.89
20630	Gl 137	G5 V	4.83			300 × 3	1.62
174719		G6 V	5.30	600 × 2			1.60
196761	Gl 796	G6 V	6.37	900			2.03
152391	Gl 641	G6 V	6.64	1200			2.01
224619		G7 V	7.64	1800			1.74
156274	Gl 666 A	G8 V	5.48	300×2 + 180			2.06
10700	52 τ Cet	G8 V	3.50	180		120 × 3	1.74
20794	Gl 139	G8 V	4.27	1200			1.67
155886	36 Oph a	K0 V	5.29	300			2.77
155885	36 Oph b	K1 V	5.33	300			2.90
22049	18 ϵ Eri	K2 V	3.73	300 + 180		300 × 2	3.18
191408	Gl 783 A	K3 V	5.32	600 + 420			2.98
50281	Gl 250 A	K3 V	6.58		1200		5.57
217580	Gl 886	K4 V	7.46	1200 + 1800		1800 × 3	4.63
131977	Gl 570 A	K4 V	5.74	2400	3600		6.48
209100	ϵ Ind	K5 V	4.69	900			5.42
196795	Gl 795	K5 V	7.89	2400			7.43
120467	Gl 529	K6 V	8.17	600	3600 × 2		9.27
209290	Gl 846	M0.5 V	9.16			1800 × 6	12.18
42581	Gl 229 A	M1 V	8.15		2700 × 2		9.40
36395	Gl 205	M1.5 V	7.97		3600		9.99
131976	Gl 570 B	M1.5 V	8.01		3600		9.86
119850	Gl 526	M2 V	8.47		3600 + 3400		8.67
180617	Gl 752 A	M3 V	9.12		2700		8.70

Table 1. (continued)

HD #	Other id.	Sp. type	V	Exposure time CAT 93	Exposure time CAT 95	Exposure time McD 94	$\langle W_\lambda \rangle$
136202	5 Ser	F8 III	5.06	60 + 300			0.93
144608	10 ω^2 Sco	G3 III	4.32	180			1.42
204381	36 Cap	G5 III	4.51	900			1.56
21120	1 o Tau	G6 III	3.60	120			1.77
126035	2 Lib	G7 III	6.21	1800			2.04
9270	99 η Psc	G8 III	3.62	150		150 × 3	1.68
10761	110 o Psc	G8 III	4.26	300			1.72
177241	39 o Sgr	G9 III	3.76	60			1.91
219615	6 γ Psc	G9 III	3.69	60			1.16
211391	43 θ Aqr	G9 III	4.16			200 + 240 × 2	2.05
163917	64 ν Oph	K0 III	3.34	2400 + 120			2.47
28	33 Psc	K0 III	4.61			300 × 3	2.22
176678	12 ι Aql	K1 III	4.02	600			2.14
18322	3 η Eri	K1 III	3.89			240 × 4	2.30
1522	8 ι Cet	K1.5 III	3.54	120			3.38
218594	88 Aqr	K1.5 III	3.66			180 × 3	2.63
140573	24 α Ser	K2 III	2.64	120 + 30			3.64
161096	60 β Oph	K2 III	2.76	30			3.50
6805	31 η Cet	K2 III	3.45			180 × 3	3.20
171443	α Sct	K3 III	3.84	180 + 60 × 2			3.16
221148	HR8924	K3 III	6.25			900 + 1500 + 1200	5.03
10824	HR513	K4 III	5.34	420			4.21
223719	22 Psc	K4 III	5.55			600 × 2	3.79
4656	63 δ Psc	K4.5 III	4.43			200 × 2	4.27
151249	η Ara	K5 III	3.76	300	1200		3.79
149447	HR6166	K6 III	4.16	300	1200		4.31
149161	29 Her	K7 III	4.84		1200		3.61
12274	59 υ Cet	M0 III	4.00	120		180 × 3	5.26
95578	61 π^2 Leo	M0 III	4.74		1200 × 2		4.72
218329	55 Peg	M1 III	4.52			300 × 3	6.34
18884	92 α Cet	M1.5 III	2.53			30 × 3	4.15
1879		M2 III	6.45			1200 × 3	4.14
117675	74 Vir	M2.5 III	4.69	1200 × 2 + 300	1200		4.06
132525	HR5584	M2.5 III	5.93		3600		5.12
133216	20 σ Lib	M2.5 III	3.30		900		2.99
198026	3 κ Aqr	M3 III	4.43	120			3.04
224935	30 Psc	M3 III	4.40	120		200 × 3	3.94
154143	HR6337	M3 III	4.98		1200		4.27
1014	HR46	M3 III	5.12			300 × 2	3.43
57615	HR2802	M3 III	5.87		2700		3.38
4408	57 Psc	M4 III	5.35	420		240 × 3	2.33
120323	2 Cen	M4.5 III	4.21		900		2.04
214952	β Gru	M5 III	2.10	5 + 20 + 35			2.32
82668	N Vel	M5 III	3.13		1800 + 360		4.16
151061		M5 III	6.90		1800		2.12

in $T_{\rm eff}$, which grows towards cooler stars, can be greater than 500 K, while the uncertainty in $\log g$ varies between 0.03 and 0.07 dex for dwarf stars, and from 0.1 to 0.7 dex for giant stars. For giants cooler than K3 the estimate of g becomes very difficult because this is the HR diagram zone where the evolutionary traces curve upwards. The grid has a temperature step of 500 K, except for models with $T_{\rm eff} < 4000$ K; these models have been computed to cover a temperature interval as wide as possible, and to test them at very low temperatures.

The photospheric models, in radiative equilibrium (RE) and local thermodynamic equilibrium (LTE), were computed using the code MARCS, developed by Bengt Gustafsson and Åke Nordlund (Gustafsson 1973; Gustafsson et al. 1975), which treats convection with the mixing length formalism and line blanketing by means of opacity distribution functions.

The model atmospheres were extended outwards, i.e. for $\log \tau_{5000}$ less than ~ -4 (where τ_{5000} is the optical depth at 5000 Å), by assuming a stellar chromosphere built by scaling that of the solar reference model MACKKL (Maltby et al. 1986). The relation for this scaling is simply

$$T^*(\tau_{5000}) = T^{\odot}(\tau_{5000}) \times T^*_{\rm eff}/T^{\odot}_{\rm eff}, \quad (1)$$

where T^* and $T^{\odot}$ are the temperatures in the chromospheres of the star and the Sun, respectively, while $T^*_{\rm eff}$ and $T^{\odot}_{\rm eff}$ (5780 K) are the stellar and solar effective temperatures. This scaling does not account for the variability of stellar activity and is compatible with our observational sample of low active stars. The final temperature vs. optical depth distributions are shown in Fig. 1 for both dwarf and giant stars.

The electron density $N_{\rm e}$ in the chromosphere was assumed to be constant and equal to its photospheric value at $\log \tau_{5000} = -4$. This simplification is justified by the very low sensitivity of W_λ to $N_{\rm e}$ in cool stars (only 7 mÅ for a variation of $\log N_{\rm e}$ equal to 0.4 dex) and by the relatively slow variation of $N_{\rm e}$ in chromospheres (Ayres 1979). Electronic density vs. optical depth distributions are shown in Fig. 2 for both dwarf and giant stars.

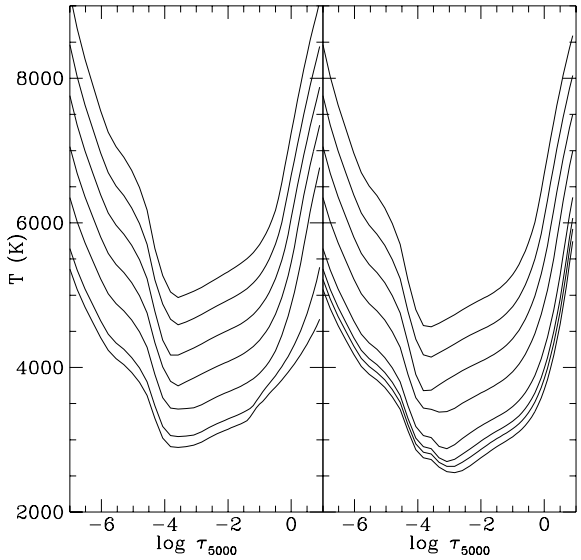

Fig. 1. Temperature vs. optical depth distributions for dwarfs (left) and giants (right).

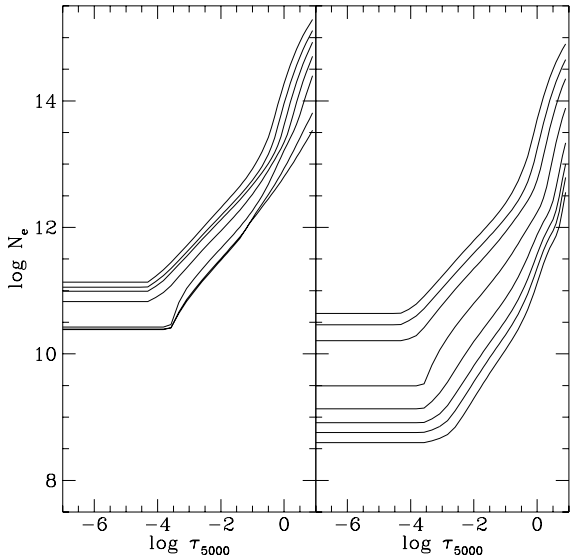

Fig. 2. Electron density vs. optical depth distributions for dwarfs (left) and giants (right). The upper curves correspond to the hotter models.

Table 2. Grid of the basic stellar parameters for late-type stars. The units for $T_{\rm eff}$ and g are K and cm s^{-2}, respectively.

DWARFS			GIANTS		
Sp. type.	$T_{\rm eff}$	log g	Sp. type.	$T_{\rm eff}$	log g
F5 V	6500	4.27	F7 III	6000	3.47
G0 V	6000	4.32	G1 III	5500	3.30
G7 V	5500	4.44	G5 III	5000	3.10
K1.5 V	5000	4.51	K1.5 III	4500	2.45
K4.5 V	4500	4.54	K4 III	4000	2.00
K8.5 V	4000	4.62	K8 III	3800	1.60
M0 V	3800	4.63	M1 III	3700	1.30
			M5 III	3600	1.00

3.2. Spectral synthesis

For the NLTE line synthesis of the Na I D equivalent widths over the grid of model atmospheres, we used the code MULTI version 2.0, implemented by Carlsson (1986), and modified by us to take into account the sodium D-line blend. In particular, we accounted for the fine structure of the upper level of the resonance transition assuming that the relative populations of the two sublevels are proportional to their degeneracies. This version of the code has a background opacity package that includes the formation of a number of diatomic molecules in the density calculations based on the program described by Gustafsson (1973) and Gustafsson et al. (1975); moreover it takes into account only inelastic collisions with electrons, neglecting those with neutral atoms (hydrogen in particular) occurring in the atmospheres of the coolest stars, which could favour an approach to the LTE condition; this is justified by the fact that these collisional rates are probably several orders of magnitude less than the corresponding rates due to electronic collisions (e.g. Caccin, Gomez & Severino 1993).

For all the models of the grid, we adopted for the microturbulence parameter ξ the value of 2 km s^{-1}, which best reproduces the observed curves of growth in the Sun (Cowley & Cowley 1964). Moreover, we used the solar global metallicity (i.e. [Fe/H] = 0) and the value log N(Na)= 6.31 for the sodium abundance (Grevesse & Anders 1991, in the usual logarithmic scale where hydrogen abundance is 12).

Fig. 3 shows the synthetic sodium profiles for dwarf and giant stars. It is apparent, as one would expect, that the sodium D resonance lines strengthen toward later spectral types by developing their Lorentzian wings, and this growth is more effective for dwarf stars than for giants where pressure broadening is reduced by the low gravity. Note the severe blending between D_1 and D_2, which justifies our treatment of line overlapping. Note also that only the coolest dwarf model produces a sodium doublet with a visible emission in the line cores, which is a result of the use of solar type chromospheres.

Fig. 4 plots computed equivalent widths of the Na I doublet (D_1 and D_2) vs. $T_{\rm eff}$. For both dwarfs and giants W_λ grows with increasing spectral type. A least-squares fit to the ($T_{\rm eff}$, W_λ) calculated data leads to the following relation:

$$\log \frac{W_\lambda}{\lambda} = a\frac{5040}{T_{\rm eff}} + b, \qquad (2)$$

where W_λ is expressed in Å λ = 5890 Å ; a = 2.52 eV, b = −5.72, and a = 1.88 eV, b = −5.37 for dwarfs and giants, respectively. W_λ depends mostly upon the abundance of neutral sodium, so a is essentially the Na I ionization potential I = 5.14 eV divided by two because the D lines are located on the damping part of the curve of growth. At a given $T_{\rm eff}$, W_λ is greater for dwarfs than for giants, because it depends on g, mainly through Van der Waals collisional broadening.

Fig. 5 shows that the differences between NLTE and LTE calculations of W_λ are smaller than 25%. At high $T_{\rm eff}$ the NLTE

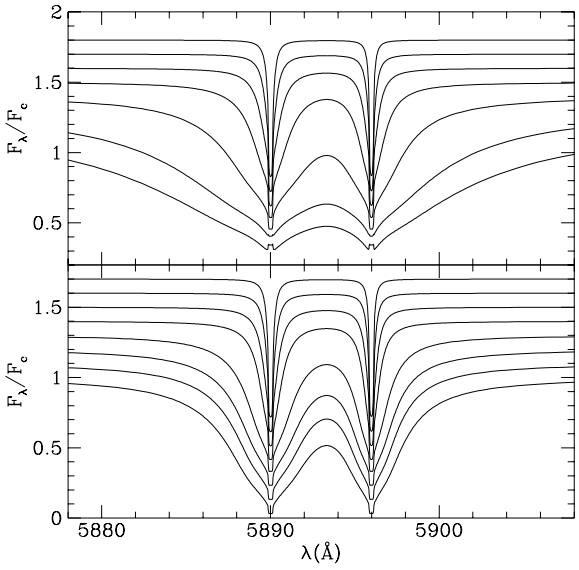

Fig. 3. Synthetic sodium profiles for dwarfs (top) and giants (bottom). The upper curves correspond to the hotter models. A constant offset has been added to each relative flux to separate the spectra vertically.

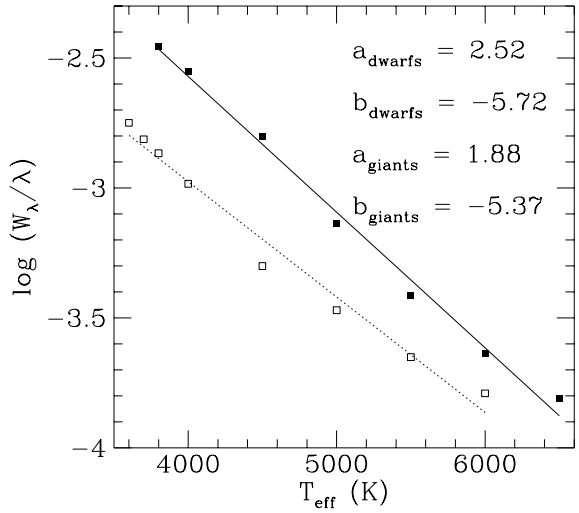

Fig. 4. Calculated W_λ vs. $T_{\rm eff}$. The solid-line plots the linear best fit for dwarfs (filled squares) and dotted line for giants (open squares).

effects, due to deviations of the line source function S_λ from the Planck function B_λ in the upper layers (where the cores of the D lines are formed), tend to increase the equivalent width with respect to that calculated in LTE (W_λ^*). At low $T_{\rm eff}$, W_λ is less sensitive to such effects because the wings predominate over the core, so that most of the lines are formed in the inner layers. Note, however, that at these temperatures the behaviour of dwarf and giant stars is different, so the NLTE equivalent width for giants can be 25 % less than that of the LTE, while the deviations for dwarfs remain positive.

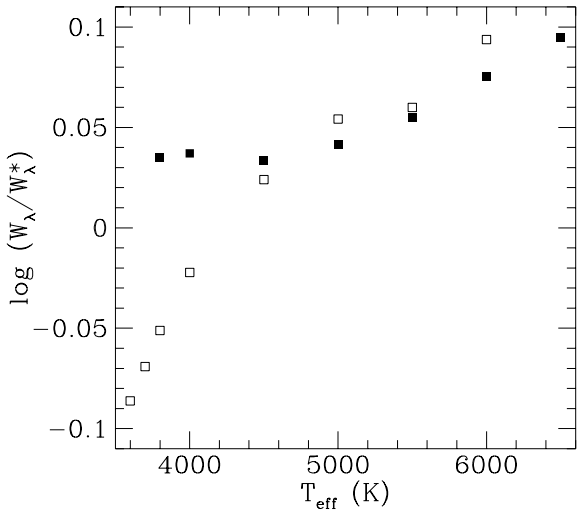

Fig. 5. NLTE effects on calculated W_λ vs. $T_{\rm eff}$ for dwarfs (filled squares) and giants (open squares). Note that W_λ^* is the equivalent width computed in LTE conditions.

4. Comparison between observed and synthetic lines

In Sect. 3 we computed W_λ vs. $T_{\rm eff}$ and $\log g$ adopting the calibration ($T_{\rm eff}$, $\log g$)–(spectral type, luminosity class) of Table 2, and solar values for ξ, metallicity and sodium abundance. The comparison between observations and model calculations is shown in Figs. 6 and 7 in the form of plots of equivalent widths vs. effective temperature.

In order to compare observed and calculated W_λ we accounted for the possible variations of the basic stellar parameters. The uncertainty on $T_{\rm eff}$ derived from different calibrations (see also Gray & Corbally 1994) is at least 250 K. A variation of $\Delta T_{\rm eff}$ = +150 K in the assumed stellar $T_{\rm eff}$ induces a decrease in W_λ of 10–20% and 10–30% for dwarfs and giants, respectively. This means that a horizontal shift of about 300 K in the observed W_λ vs. $T_{\rm eff}$ curve is sufficient to obtain an agreement between observed and computed W_λ for $T_{\rm eff} > 4000$ K. The second considered quantity is gravity, which is not an easy parameter to estimate, especially for red giants. Typical uncertainties are in the range 0.2–0.3 dex. Fortunately, W_λ is not very sensitive to differences of this order. The uncertainty on ξ may be of the order of $\pm$0.5 km s^{-1}. On the other hand, even a change of $\Delta\xi = -1$ km s^{-1} does not affect significantly W$_\lambda$. Variations of global metallicity can have effects both on atmospheric and atomic models. However, a change of [Fe/H] = -0.5 dex leads to negligible differences in solar-type model atmospheres (see also Gustafsson et al. 1975). We then used the models of Sect. 3 to recalculate W_λ using a different sodium abundance ($\Delta \log N$(Na) = -0.48 dex) finding induced uncertainties as high as 30–40%.

By taking into account both experimental errors and possible variations of the stellar parameters, the comparison between observations and theoretical calculations allows us to state that for $T_{\rm eff} > 4000$ K the model atmospheres we have used are

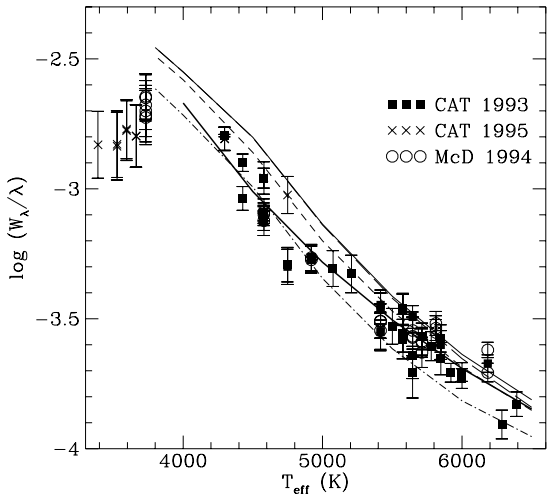

Fig. 6. Comparison between observed and computed equivalent widths for dwarfs as a function of the effective temperature. Observed data are represented with different symbols according to the observing runs, as indicated in the panel. The thick line represents the fit of experimental data for $T_{\rm eff} > 4000$ K, with $a = 2.43$ eV and $b = -5.73$ (Eq. 2). The other lines refer to our model calculations: the solid, light line corresponds to the adopted calibration ($T_{\rm eff}$, $\log g$, ξ, [Na/H])–(spectral type, luminosity class); dotted and dashed lines show the effect of a variation of $\Delta \log g = -0.25$ dex (short dash), $\Delta\xi = -1$ km s^{-1} (long dash), and $\Delta \log N({\rm Na}) = -0.48$ dex (dot-short dash), respectively. Note that the effect of $\Delta\xi$ is small, and therefore the long dash line is generally overlain by the solid, light line.

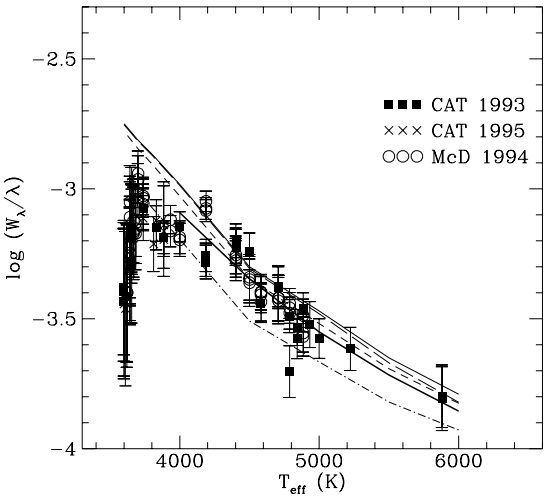

Fig. 7. The same as in Fig. 6, but for giants, and with $a = 1.82$ eV and $b = -5.38$ in the fit of the experimental data (Eq. 2).

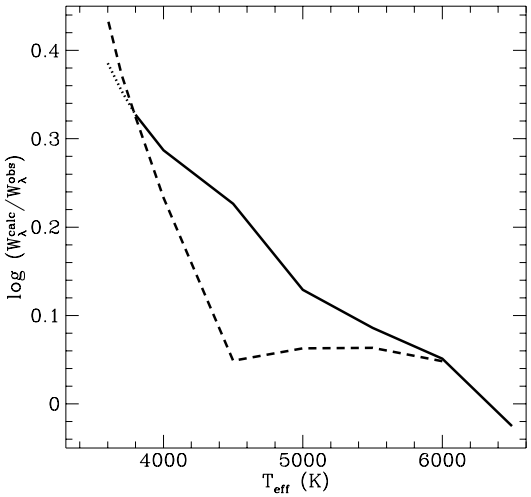

Fig. 8. Difference between computed and observed equivalent widths for dwarfs (solid line; dotted line for low temperatures where the curve has been extrapolated) and giants (dashed line). Calculations were made using the models of Sect. 3; observational data were fitted with a third-order polynomial.

able to reproduce the observations for both luminosity classes. In this restricted temperature range the best fit to the observed data with Eq. 2 gives $a = 2.43$ eV, $b = -5.73$ and $a = 1.82$ eV, $b = -5.38$ for dwarfs and giants, respectively.

For the M-type stars, i.e. the coolest stars in our sample, the theoretical calculations overstimate the observations by about $0.3 - 0.5$ dex. For a better evaluation of this discrepancy, the mean difference between computed and observed W_λ is plotted as a function of $T_{\rm eff}$ in Fig. 8: it is apparent that the lower the temperature, the larger the difference.

In fact, at low temperatures there is an inversion in the trend of the observed W_λ, i.e. W_λ becomes smaller with decreasing $T_{\rm eff}$, which is contrary to the behaviour of the calculations. The existence of this discrepancy, which is too large to be considered as due to uncertainties in the stellar parameters, led us to rediscuss the kind of background opacities we have used for the spectral synthesis (see Sect. 3.2). For cooler models there are certainly still missing opacities. Considerable progress has been made recently in the modeling of early M-giant spectra (e.g. Plez et al. 1992) as well as M-dwarf spectra (e.g. Allard et al. 1994; Allard & Hauschildt 1995; Kirkpatrick et al. 1993). However, further improvements are still needed for both dwarf and giant models.

In their careful theoretical analysis of the Na I resonance doublet as chromospheric diagnostics in a typical M dwarf ($T_{\rm eff} = 3700$ K, $\log g = 4.7$ and solar metallicity) with different levels of chromospheric activity, Andretta et al. (1997) add to the "standard" MULTI calculations, opacities from atomic and molecular lines provided by Allard & Hauschildt.

From the inspection of their Figs. 4 and 14, we see that: *i*) the inclusion of this additional opacity produces significant variations in the "background" photospheric flux, which Andretta et al. define as the emerging spectrum obtained ignoring line absorption by sodium atoms, and *ii*) there is a large difference between the sodium-line profiles (in absolute units) computed taking into account background line opacities or continuum opacities only.

This example clearly demonstrates that an improved comparison with observations of M-star equivalent widths should

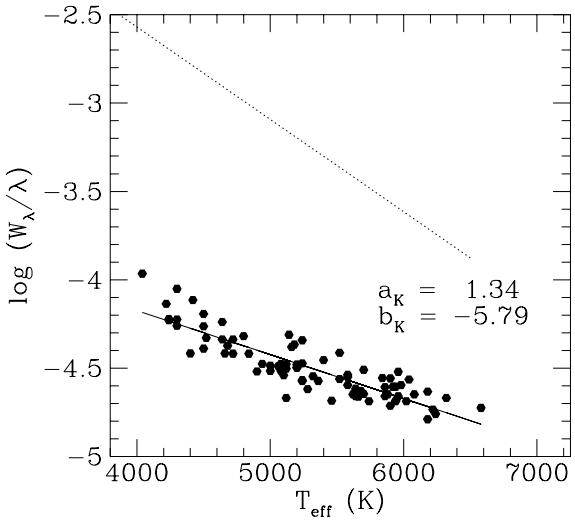

Fig. 9. Observed W_λ vs. $T_{\rm eff}$ for the K I λ 7699 Å line in Pleiades cool dwarfs (Soderblom et al. 1993). The solid line represents a least-squares fit for stars with $T_{\rm eff} > 4000$ K; a and b are the coefficients of Eq. 2; the dotted line represents the theoretical Na relation for dwarfs.

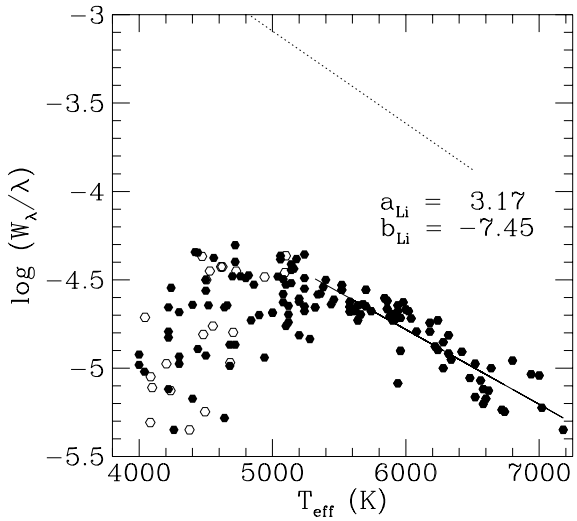

Fig. 10. Observed W_λ vs $T_{\rm eff}$ for the Li I λ 6708 Å line in Pleiades cool dwarfs (filled circles: Soderblom et al. 1993; open circles: García López et al. 1994). The solid line represents a least-squares fit for stars with $T_{\rm eff} > 5500$ K; a and b are the coefficients of Eq. 2; the dotted line represents the Na theoretical relation for dwarfs.

include a realistic treatment of the background opacity. On the other hand, the low wavelength resolution (2 Å) of the opacity table used in their calculations does not allow us to infer a quantitative estimate of the effect due to line blanketing (useful for our analysis of high-resolution sodium spectra), neither can we conclude on a firm basis that this effect would substantially reduce the discrepancy shown in Fig. 8.

Furthermore we have compared our computed and observed W_λ vs. $T_{\rm eff}$ relations for Na I D lines, with those observed by Soderblom et al. (1993) for the K I λ 7699 Å line, and from Soderblom et al. and García López et al. (1994) for the Li I λ 6708 Å line, in a sample of Pleiades cool dwarfs. These are both resonance lines of neutral alkalis, so they all should be formed under conditions similar to the Na I doublet. In order to have a linear relation for observed log W_λ vs. $T_{\rm eff}^{-1}$ as in Eq. 2, a least-squares fit has been calculated using stars with $T_{\rm eff} > 4000$ K and $T_{\rm eff} > 5500$ K for K and Li, respectively. We have avoided using stars cooler than 5000 K for the Li fit, due to the strong Li depletion which has taken place in those stars. The resulting fits are plotted in Figs. 9 and 10. The theoretical Na relation for dwarfs is also plotted, and the comparison shows that the greater the ionization potential, the steeper is the line represented by Eq. 2 (a = 1.34 eV, I = 4.34 eV for K; a = 3.17 eV, I = 5.39 eV for Li), and that the theoretical Na curve is about 1 dex higher than both K and Li fits. This confirms that ionization plays an important role in fixing the W_λ vs. $T_{\rm eff}$ relation, although a complete analysis would require also the consideration of other effects, such as the temperature dependence of the continuum absorption coefficient, the different position of K I and Li I lines on the corresponding curve of growth, and the NLTE effects.

5. Conclusions

We have obtained observed W_λ vs. $T_{\rm eff}$ relations (W_λ being the total equivalent width of the Na I doublet) for a wide sample of late-type dwarf and giant stars. Equivalent theoretical relations have been computed using model atmospheres which include the photosphere and low chromosphere, and taking into account the NLTE effects on the line formation.

The increasing broadening of the sodium doublet with decreasing effective temperature plays a major role in determining the theoretical equivalent widths. Accordingly, the electronic density of the model does not affect the equivalent width, because the Stark broadening is negligible with respect to the Van der Waals broadening. Moreover, the chromospheric part of the model is not very important, in particular for the coolest stars, because it might modify only the cores of the D lines, which give a small contribution to the strength of the doublet. On the other side, when the wings are not yet fully developed, as it occurs in the solar case, the doublet is photoionization dominated, and, therefore, the details of the chromospheric temperature rise are unimportant again. The analysis of the variations produced by perturbing the stellar model parameters, shows that the theoretical equivalent widths are strongly affected by variations in sodium abundance and effective temperature, to a small extent by variations in surface gravity, and are almost insensitive to variations of the microturbulence parameter.

A good agreement has been found between observed and theoretical W_λ vs. $T_{\rm eff}$ relations for dwarf and giant stars with effective temperatures greater than 4000 K, showing that the models are able to reproduce the Na I D lines formed throughout the photosphere and low chromosphere of these stars. However, the same models overestimate W_λ at lower effective tempera-

tures. Possible uncertainties in the model parameters together with experimental errors in measuring the stellar equivalent widths, are not sufficient to explain such a large discrepancy. Moreover, a possible reduction of NLTE effects, due for instance to a contribution of b-b collisions with neutral hydrogen which have been neglected in our calculations would enhance the difference between observations and calculations.

We have discussed in some detail the lack of line blanketing in the opacity package used for the spectral synthesis, mainly referring to the work of Andretta et al. (1997). At present, we cannot conclude that this effect would substantially reduce the discrepancy between observed and computed equivalent widths for M stars. However it is apparent that the inclusion in the calculation of detailed atomic and molecular opacities such as those produced by Allard, Hauschildt and collaborators is a prerequisite for any reliable spectral analysis of these cool stars.

Finally, a comparison has been made with the dependence on effective temperature of other neutral alkali (K and Li) features, in order to find some useful similarities. It appears that studying the formation of sodium lines could be helpful for a better understanding of the formation of lithium lines in late-type stars. An extension of the present work to the K I λ 7699 Å line in a similar sample of stars will be presented in a forthcoming paper.

Acknowledgements. We thank the following people for their contribution to this work: M.T. Gomez, for a number of stimulating discussions, V. Andretta for his useful comments, and J.M. Alcalá for helpful suggestions about the data analysis and for providing us with his MIDAS procedures for spectroscopic data reduction; finally we thank the anonymous referee for his helpful remarks.

References

Allard F., Hauschildt P. H., Miller S., Tennyson J., 1994, ApJ 426, L39
Allard F., Hauschildt P. H., 1995, ApJ 445, 433
Allen C. W., 1973, Astrophysical Quantities 3rd ed.). Athlone Press, London
Andretta V., Doyle J. G., Byrne P. B., 1997 A&A (in press)
Ayres T. R., 1979, ApJ 228, 509
Balachandran S., 1994, in 8th Cambridge Workshop on Cool Stars, Stellar Systems, and the Sun, J.-P. Caillault (ed.), PASPC 64, p. 234.
Caccin B., Gomez M. T., Severino G., 1993, A&A 276, 219
Carlsson M., 1986, A Computer Program for Solving Multi-Level Non-LTE Radiative Transfer Problems in Moving or Static Atmospheres, Report No. 33, Uppsala Astronomical Observatory
Covino E., Gomez M. T., Severino G., Franchini M., 1993, PASPC 40, 190
Cowley C. R., Cowley A. P., 1964, ApJ 140, 713
García López R. J., Rebolo R., Martín E. L., 1994, A&A 282, 518
Gray D. F., 1989, in FGK Stars and T Tauri Stars, NASA SP–502, p. 7, L. E. Cram and L. V. Kuhi (eds.), Monograph Series on nonthermal phenomena in stellar atmospheres
Gray R. O., Corbally C. J., 1994, AJ 107(2), 742
Grevesse N., Anders E., 1991, in Solar Interior and Atmosphere, A. N. Cox, W. C. Livingston, M. S. Matthews (eds.), p. 1227
Gustafsson B., 1973, Uppsala Astr. Obs. Ann., Band 5, No. 6
Gustafsson B., Bell R. A., Eriksson K., Nordlund Å., 1975, A&A 42, 407
Gustafsson B., Jørgensen U. G., 1994, A&AR 6, 19
Kirkpatrick J. D., Kelly D. M., Rieke G. H., et al., 1993, ApJ 402, 643
Lindgren H., Gilliotte A., 1989, ESO Operating Manual No. 8
Maltby P., Avrett E. H., Carlsson M., et al., 1986, ApJ 306, 284
Plez B., Brett J. M., Nordlund Å., 1992, A&A 256, 551
Schmidt-Kaler Th., 1982, in Landolt-Börnstein: Numerical Data and Functional Relationships in Science and Tecnology, New Series, Group VI, Volume 2, K. Schaifers and H.H. Voigt (eds.), p. 1
Severino G., Gomez M. T., Caccin B., 1994, Solar Surface Magnetism, NATO ASI Series C433, 169
Soderblom D. R., Jones B. F., Balachandran S., et al., 1993, AJ 106(3), 1059
Tripicchio A., Covino E., Gomez M. T., Severino G., Terranegra L., 1996, in 9th Cambridge Workshop on Cool Stars, Stellar Systems, and the Sun, R. Pallavicini & A. K. Dupree (eds.), PASPC 109, 575
Tull R. G., MacQueen P. J., Sneden C., Lambert D. L., 1995, PASP 107, 251

This article was processed by the author using Springer-Verlag LaTeX A&A style file *L-AA* version 3.